Assembly and Disassembly Kinetics of Anthrax Toxin Complexes†

Kenneth A. Christensen,‡,§ Bryan A. Krantz,‡ and R. John Collier*,‡

Department of Microbiology and Molecular Genetics, Harvard Medical School, Boston, Massachusetts 02115, and Department of Chemistry, Clemson University, Clemson, South Carolina 29634

Received September 9, 2005; Revised Manuscript Received December 9, 2005

ABSTRACT: Proteolytic activation of the protective antigen (PA) component of anthrax toxin allows it to self-associate into a ring-shaped homoheptamer, $[PA_{63}]_7$, which can bind the enzymatic components lethal factor (LF) and edema factor (EF). $[PA_{63}]_7$ is a pore-precursor (prepore), and under the low-pH conditions of the endosome, it forms a transmembrane pore that allows LF and EF to enter the cytosol. PA was labeled with donor and acceptor fluorescent dyes, and Förster resonance energy transfer was used to measure the assembly and disassembly kinetics of the prepore complex in solution. The dissociation rate constant for $[PA_{63}]_7$ was 1×10^{-6} s^{-1} ($t_{1/2} \sim 7$ days). In contrast, a ternary complex containing the PA-binding domain of LF (LF_N) bound to a PA_{63} dimer composed of two nonoligomerizing mutants dissociated rapidly ($t_{1/2} \sim 1$ min). Thus, the substantial decrease in the rate of disassembly of $[PA_{63}]_7$ relative to the ternary complex is due to the cooperative interactions among neighboring subunits in the heptameric ring. Low concentrations of LF_N promoted assembly of the prepore from proteolytically activated PA, whereas high concentrations inhibited assembly of both the prepore and the ternary complex. A self-assembly scheme of anthrax toxin complexes is proposed.

Anthrax toxin, a major virulence factor of *Bacillus anthracis*, consists of three nontoxic proteins that interact at the mammalian cell surface or in solution to form toxic noncovalent complexes (*1*, *2*). The three proteins are edema factor (EF),[1] a calmodulin-dependent adenylate cyclase; lethal factor (LF), a Zn^{2+}-metalloprotease; and protective antigen (PA_{83}, 83 kDa), a nonenzymatic protein that, after proteolytic activation, can bind EF and LF and deliver them to the cytosol of mammalian cells. Once within the cytosol, EF and LF catalyze reactions that cause deleterious effects on the host (*3*−*5*).

The following model of anthrax toxin assembly and action at the cellular level has emerged in recent years. PA_{83} binds to either of two known cell surface receptor proteins (*6*, *7*). A cellular protease of the furin family then cleaves PA_{83} into a "nicked" form (nPA_{83}) containing two fragments: PA_{20} (20 kDa), corresponding to the N terminus, and PA_{63} (63 kDa), corresponding to the C terminus (*8*, *9*). PA_{20} dissociates into the medium and plays no further known role in toxin action. Its removal eliminates a steric barrier to self-association of PA_{63}, allowing this fragment to oligomerize and form a heptameric ring-shaped structure, $[PA_{63}]_7$, termed the prepore (*10*). The PA_{63} prepore is able to bind up to three molecules of LF and/or EF competitively and with nanomolar affinity (*11*, *12*). The resulting complexes are localized to detergent-resistant lipid microdomains, where they undergo receptor-mediated endocytosis (*13*). Acidification of the toxin-containing compartment causes a structural rearrangement of the prepore that enables it to insert into the membrane and form a pore (*14*, *15*). Pore formation is linked to translocation of the bound enzymatic cargo (LF or EF) to the cytosol by an acid-induced unfolding mechanism (*16*−*18*). LF cleaves members of the mitogen-activated protein kinase kinase family (*4*, *5*), leading by a still poorly defined sequence of events to host cell death. Elevation of the cAMP concentration by EF protects the bacteria from phagocytic destruction (*19*).

The assembly of toxic complexes from PA, EF, and LF can be replicated in solution when trypsin or a serum protease is used to activate PA (*14*). In the absence of EF or LF, the

† This work was supported by NIH Grant R37-A1022021 (R.J.C.).

* Corresponding author [e-mail jcollier@hms.harvard.edu; telephone (617) 432-1930; fax (617) 432-0115].

‡ Harvard Medical School.

§ Clemson University.

[1] Abbreviations: PA, protective antigen; $[PA_{63}]_7$, protective antigen homoheptamer; LF, lethal factor; EF, edema factor; LF_N, lethal factor N-terminal domain; PA_{83}, 83 kDa full-length protective antigen; nPA_{83}, nicked protective antigen (83 kDa); PA_{20}, 20 kDa N-terminal fragment of protective antigen; PA_{63}, 63 kDa C-terminal fragment of protective antigen; EF_N, edema factor N-terminal domain; FRET, Förster resonance energy transfer; cAMP, cyclic adenosine monophosphate; TPCK, L-1-tosylamide-2-phenylethylchloromethyl ketone; IPTG, isopropyl β-D-thiogalactoside; DTT, dithiothreitol; nPA_{83} K563C*488, nicked protective antigen, residue 563 labeled with Alexa fluor 488 C_5 maleimide; nPA_{83} K563C*546, nicked protective antigen, residue 563 labeled with Alexa fluor 546 C_5 maleimide; nPA_{83} K563C*594, nicked protective antigen, residue 563 labeled with Alexa fluor 594 C_5 maleimide; $[PA_{63}]_7$*FRET, protective antigen homoheptamer containing a 1:1 ratio of protective antigen where residue 563 is labeled with Alexa fluor 488 plus either Alexa fluor 546 or 594; GdmHCl, guanidine−HCl; $[PA_{63}]_2$·LF_N, ternary complex of 1:1 ratio of protective antigen nonoligomerizing mutants (D512K and K199E R468A R470D) plus the N-terminal domain of lethal factor; nPA_{83} D512K K563C*488, nonoligomerizing protective antigen mutant, residue 563 labeled with Alexa fluor 488; nPA_{83} K199E R468A R470D K563C*546, nonoligomerizing protective antigen mutant, residue 563 labeled with Alexa fluor 546; $[PA_{63}]_2$·LF_N*FRET, protective antigen ternary complex with the lethal factor N-terminal domain labeled at protective antigen residue 563 with Alexa fluor 488 and 546; $[PA_{63}]7$·$(LF_N)_3$, protective antigen homoheptamer saturated with N-terminal domain of lethal factor ligands; LF_N E126C*594, N-terminal domain of lethal factor, residue 126 labeled with Alexa fluor 594 C_5 maleimide; PA_{63}·LF_N, putative 1:1 complex with protective antigen and LF_N; k_d, dissociation rate constant; k_a, association rate constant; DN, protective antigen mutant that displays dominant negative phenotype; K_d, equilibrium dissociation constant; Cys, cysteine.

10.1021/bi051830y CCC: $33.50
Published on Web 01/31/2006

PA_{20} and PA_{63} fragments tend to remain associated via noncovalent interactions [equilibrium dissociation constant ≈ 190 nM (*20*)]. When PA_{63} is separated from PA_{20} by anion-exchange chromatography of nPA_{83}, it spontaneously oligomerizes to the prepore state (*14*). Alternatively, oligomerization of PA_{63} can be stimulated by adding LF, EF, or their PA_{63}-binding N-terminal domains (LF_N and EF_N, respectively) to nPA_{83} in solution (*21*, *22*). As no quantitative study of PA_{63} oligomerization or dissociation has been reported, we describe here measurements of the kinetics of PA_{63} oligomer formation and dissociation in solution.

MATERIALS AND METHODS

Protein Expression and Purification. PA_{83} (K563C, D512K K563C, K199E R468A R470D K563C) and LF_N (residues 1−263 of LF) were produced recombinantly in *Escherichia coli* BL-21 DE3 Star using the pET 22b expression system for PA_{83} and the pET 15b expression system for LF_N as described previously (*22*). Briefly, the proteins were expressed in cultures grown in a 5-L fermentor using ECPM1 medium supplemented with 50 mg/L carbenicillin until an OD_{600} of 3−10 was reached (*22*, *23*). The cultures were induced with IPTG (0.8−1 mM) for 3−4 h at 27−30 °C for PA_{83} and at 37 °C for LF_N until a final OD_{600} of 6−20 was reached. Periplasmic lysates were buffered with 20 mM Tris-Cl (pH 8.5) and supplemented with 2 mM dithiothreitol to prevent oxidation of the Cys residues. PA_{83} was purified by anion-exchange chromatography (Q Sepharose) with a 0−250 mM NaCl gradient using buffers A (20 mM Tris-Cl, 1 mM $CaCl_2$, pH 8.5) and B (A + 1 M NaCl). Hexahistadine-tagged LF_N was purified from cell pellets lysed by French press and sonication using Ni^{2+} affinity chromatography (*24*). Pure fractions, as determined by SDS−PAGE, were concentrated and stored at −80 °C. Protein concentrations were determined by absorbance spectrophotometry [ϵ_{280} (PA_{83}) 75 670 M^{-1} cm^{-1} and (LF_N) 18 040 M^{-1} cm^{-1}].

Preparation of nPA_{83} and $[PA_{63}]_7$. Nicked PA_{83} (nPA_{83}) was prepared using TPCK-treated trypsin (Sigma) by incubating PA_{83} (1−2 mg/mL) in buffer C (A + 150 mM NaCl) for 35 min at room temperature at a 1:1000 w/w ratio of trypsin to PA_{83} followed by the addition of a 1:100 w/w ratio of soybean trypsin inhibitor (Sigma) to prevent further proteolysis. This procedure yielded a >90% nicking efficiency. $[PA_{63}]_7$ was prepared at >95% purity using anion-exchange chromatography. Briefly, nPA_{83} was loaded onto the column (Q Sepharose) followed by elution using a 0−500 mM NaCl gradient with buffers A and B. Separation of PA_{20} from PA_{63} was followed by spontaneous oligomerization of PA_{63} on column. Pure fractions, as determined by SDS−PAGE, were concentrated and stored at −80 °C. $[PA_{63}]_7$ concentrations were determined by absorbance spectrophotometry (ϵ_{280} 347 480 M^{-1} cm^{-1}).

Fluorescent Labeling of Proteins. Proteins with single Cys mutations were labeled with Alexa fluor 488 C_5 maleimide, Alexa fluor 546 C_5 maleimide, or Alexa fluor 594 C_5 maleimide (Invitrogen) using the manufacturer's procedures. Protein solutions were exchanged back into buffer C by gel filtration. The protein conjugates' dye-to-protein ratios were 0.9−1.2 as determined by absorbance spectrophotometry. Dye-labeled proteins were stored at −80 °C.

Measurements of k_d for $[PA_{63}]_7$. $[PA_{63}]_7$ was purified from a 1:1 mixture of nPA_{83} K563C labeled with Alexa fluor 488 (nPA_{83} K563C*488) and nPA_{83} K563C labeled with Alexa fluor 546 or Alexa fluor 594 (nPA_{83} K563C*564, nPA_{83} K563C*594). The purified $[PA_{63}]_7$ contained both donor and acceptor labels ($[PA_{63}]_7$*FRET). For rapid dilution experiments, $[PA_{63}]_7$*FRET was diluted from 10 μM to 10 nM in buffer D (50 mM Tris-Cl, pH 8.5, 150 mM NaCl, 0.5 mg/mL BSA, and 0.02% NaN_3). In competition experiments, 10 nM labeled $[PA_{63}]_7$*FRET and 250 nM unlabeled $[PA_{63}]_7$ were combined in buffer D. In both experiments, the fluorescence emission ratio (570/525 ± 10 nm emission, 488 ± 4 nm excitation from Xe arc lamp) was monitored using a spectrofluorometer over 16 days. Solution temperatures were ∼20 °C throughout the entire experiment. Data were fit to a single-exponential decay model using nonlinear least squares to recover the observed dissociation constant, k_d.

Additional experiments contained the protein denaturant guanidine−HCl (GdmHCl). Various amounts of GdmHCl (0−0.6 M, as determined by refractive index) were added to 10 nM heptamer solutions in buffer D. The fluorescence emission ratio (615/525 ± 16 nm emission, 488 nm excitation from Ar^+ laser) was monitored using a spectrofluorometer over 10 days. All solutions were maintained at 20 °C throughout the entire experiment. Data were fit to a single-exponential decay model using nonlinear least squares to recover the observed dissociation constant, k_d.

Because measurements of k_d required long incubation periods at room temperature, all solutions were sterile filtered and supplemented with 0.02% NaN_3 to inhibit microbial growth that could lead to degradation of the non-covalent protein complexes. SDS−PAGE was used to monitor PA_{63} proteolysis over a 16 day period. Briefly, a 20 nM solution of $[(PA_{63})_7]$*488 in buffer D was incubated at either ∼20 or −20 °C for 16 days. At the conclusion of this period, the room temperature incubated sample was again frozen at −20 °C until electrophoresis. These solutions were loaded onto a 4−20% polyacrylamide gel. The gel was washed in ddH_2O and observed on a UV transilluminator to excite the Alexa dye without fixing or staining, which quenches the fluorescence.

Measurements of k_d for $[(PA_{63})_2{\cdot}LF_N]$ Ternary Complex. $[(PA_{63})_2{\cdot}LF_N]$ was prepared by incubating a 1:1:1 mixture of nPA_{83} D512K K563C labeled with Alexa fluor 488 (nPA_{83} D512K K563C*488), nPA_{83} K199E R468A R470D K563C labeled with Alexa 546 (nPA_{83} K199E R468A R470D K563C*546), and LF_N at 5 μM (total nPA_{83} was 10 μM). All $[(PA_{63})_2{\cdot}LF_N]$ contained both donor and acceptor labels ($[(PA_{63})_2{\cdot}LF_N]$*FRET). $[(PA_{63})_2{\cdot}LF_N]$*FRET was diluted from 5 μM to 10 nM in buffer D and the fluorescence emission ratio measured over time (570/525 ± 16 nm emission, 488 nm Ar^+ laser line excitation). The kinetic transients were fit to a single-exponential decay model (eq 1) using nonlinear least-squares analysis to recover the observed rate constant, k_d, where the amplitude at time 0, *A*, decays with respect to time, *t*. The offset, *C*, is the final value reached when the system achieves equilibrium.

$$A(t) = A\,e^{-kt} + C \tag{1}$$

Measurement of k_a for $[(PA_{63})_7{\cdot}(LF_N)_3]$ and $[(PA_{63})_2{\cdot}LF_N]$. Association rates of $[(PA_{63})_7{\cdot}(LF_N)_3]$ were determined by mixing 1:1 ratios of nPA_{83} K563C*488 and nPA_{83} K563C*594 at concentrations between 1.2 and 120 nM, followed by the

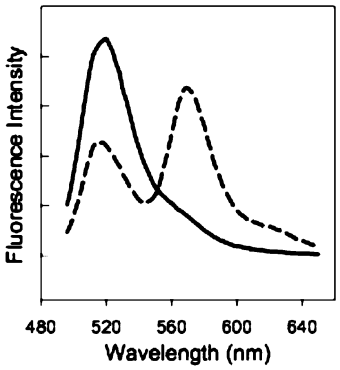

FIGURE 1: Fluorescence emission spectra of $[PA_{63}]_7$*FRET and PA_{83} control. The fluorescence emission spectrum of $[PA_{63}]_7$*FRET (100 nM; dashed line) was prepared by mixing equal parts nPA_{83} K563C*488 + nPA_{83} K563C*546 and allowing it to oligomerize on an anion-exchange column followed by purification from PA_{83} and PA_{20}. The fluorescence emission spectrum of PA_{83} was prepared by mixing equal parts PA_{83} K563C*488 and PA_{83} K563C*546 (100 nM total PA_{83}; solid line). Excitation used the 488 nm line of an Ar^+ laser. Emission band-pass was 8 nm for both spectra.

addition of variable concentrations of LF_N (from 1×10^{-9} to 1×10^{-5} M) to prompt oligomerization in solution. Oligomerization was monitored by measuring sensitized emission (FRET) via a fluorescence emission ratio of intensity (615 nm/525 nm). Similarly, association rates were determined for $[(PA_{63})_2 \cdot LF_N]$ by mixing 1:1 ratios of nPA_{83} D512K K563C*488 and nPA_{83} K199E R468A R470D K563C*546 at concentrations between 1.2 and 120 nM, followed by the addition of variable concentrations of LF_N (from 1×10^{-9} to 1×10^{-5} M) to prompt complex formation in solution. $[(PA_{63})_2 \cdot LF_N]$ formation was monitored by measuring the sensitized emission (FRET) via a fluorescence emission ratio (570 nm/525 nm $\pm$ 16 nm). All data were fit using nonlinear least-squares analysis to a second-order exponential decay model (eq 2), where the amplitude at time 0, *A*, decays with respect to time, *t* (*22*). The offset, *C*, is the final value reached when the system achieves equilibrium.

$$A(t) = A/(1 + k_a t) + C \quad (2)$$

RESULTS

Dissociation Kinetics of $[PA_{63}]_7$. Equal parts of two differently labeled PA_{83} mutants, PA_{83} K563C*488 and PA_{83} K563C*546 (or PA_{83} K563C*594), were combined, proteolytically activated with trypsin, and loaded onto an anion-exchange column. FRET-labeled $[PA_{63}]_7$ ($[PA_{63}]_7$*FRET) was isolated by gradient elution and found to show significant FRET (Figure 1, dashed line) compared to the control of an unnicked equimolar mixture of donor and acceptor labeled PA_{83} (Figure 1, solid line). The dissociation rate constant (k_d) of $[PA_{63}]_7$*FRET was measured after dilution of the complex from 10 μM to 10 nM. The decline in FRET as a function of time was monitored over 16 days, with the fluorescence emission ratio (570 nm/525 nm, 488 nm excitation) serving as the metric. We fit the observed kinetic transients (Figure 2A) to a single-exponential decay function (eq 1) and calculated the k_d to be $(1 \pm 1) \times 10^{-6}$ s^{-1}, corresponding to a $t_{1/2}$ of 7 days. When a 25-fold excess (250 nM) of unlabeled $[PA_{63}]_7$ was present, the results were indistinguishable from those obtained in the absence of the unlabeled protein (Figure 2B).

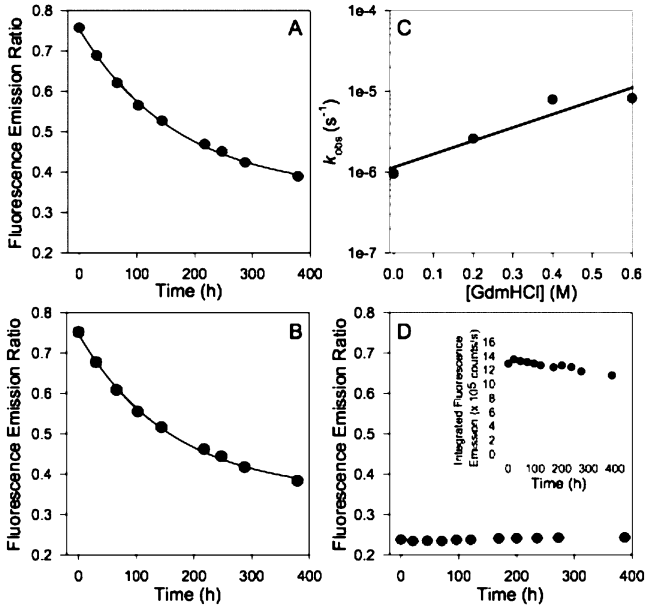

FIGURE 2: Dissociation of $[PA_{63}]_7$*FRET. (A) Rapid dilution of $[PA_{63}]_7$*FRET from 10 μM to a final concentration of 10 nM. Dissociation (decrease in FRET) was monitored over time by measuring the fluorescence emission ratio (570 nm/520 nm; 488 nm excitation). Error bars represent 95% cl. (B) Competition of 10 nM $[PA_{63}]_7$*FRET with 200 nM unlabeled $[PA_{63}]_7$. Dissociation (decrease in FRET) was monitored over time by measuring the fluorescence emission ratio (570 nm/520 nm; 488 nm excitation). Error bars represent 95% cl. (C) Plot of recovered k_d versus [GdmHCl] for the rapid dilution of $[PA_{63}]_7$*FRET with low concentrations of GdmHCl (0−0.6 M) added to accelerate the observed dissociation rate. (D) Controls: the fluorescence emission ratio of an equimolar mixture of PA_{83} K563C*488 and PA_{83} K563C*546 (unnicked) was monitored over time. (Inset) Integrated intensity over the course of an experiment. Error bars for both controls represent the 95% cl. All experimental kinetic transients were fitted to a single-exponential decay model to recover k_d. All experiments were conducted at 20 °C.

We also performed dilution experiments in the presence of low concentrations of GdmHCl to check the accuracy of the measured value of k_d. $[PA_{63}]_7$*FRET was diluted from 10 μM to 10 nM in solutions of 0.2−0.6 mM GdmHCl, and the loss of FRET due to complex dissociation was monitored, as before. The low concentrations of GdmHCl employed accelerated the rate of dissociation (the majority of signal change occurred during the first 2−4 days) while avoiding protein unfolding. The observed kinetic transients were fitted to a single-exponential decay function to recover k_d, and the rate constants were plotted versus GdmHCl concentration (Figure 2C). Extrapolating kinetics data to 0 M GdmHCl yielded a value of k_d for $[PA_{63}]_7$ identical to that determined in the absence of GdmHCl. This agreement suggested that proteolysis was not likely to contribute significantly to the observed kinetics. Additional support for this came from SDS−PAGE (Figure 3) of $[(PA_{63})_7]$*488 that had been incubated at room temperature for 16 days and a control that was stored at −20 °C during the experiment. Figure 3 shows showed that there was little change of intact PA_{63} following the long incubation. To minimize proteolysis, all solutions had been sterile filtered and supplemented with 0.02% NaN_3 to inhibit microbial growth.

To obtain a baseline for the observed changes in FRET, we mixed equal parts of unnicked PA_{83} K563C*488 and PA_{83} K563C*546 and monitored the fluorescence emission ratio

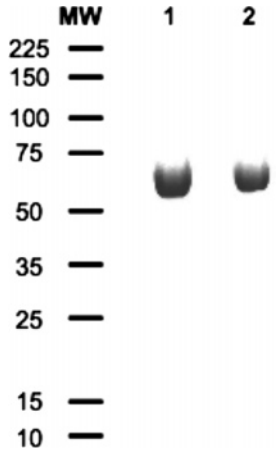

FIGURE 3: SDS−PAGE of [$(PA_{63})_7$]*488 incubated in buffer D for 16 days with MW markers indicated in kDa at left: room temperature incubation (lane 1); −20 °C storage (lane 2).

over time. Consistent with the inability of PA_{83} to self-associate, the fluorescence emission ratio was in the limit of no detectable $[PA_{63}]_7$ in solution and was stable over the time course of the experiment. Also, changes in fluorescence emission intensity were minimal (<10%) over 400 h, indicating that losses to adsorption to cuvette walls were negligible (Figure 2D, inset). Small changes in total emission intensity over time did not affect kinetics values, as they were calculated from the ratio of fluorescence emission intensities.

Association Kinetics of $[PA_{63}]_7$·LF_N. Because the equilibrium of PA_{63} oligomerization is so strongly in favor of $[PA_{63}]_7$, neither monomeric PA_{63} nor subheptameric oligomers of the wild-type fragment have ever been isolated. Hence, it has not been possible to study the kinetics of PA_{63} association in a homogeneous system (*20*). Nonetheless, LF or EF, or their N-terminal PA_{63}-binding domains, promote oligomerization of PA_{63}, starting with nPA_{83}, presumably by displacing PA_{20} and bridging associated PA_{63} subunits. Therefore, we chose to examine the oligomerization process in the presence of LF_N. Various concentrations of LF_N (from 10 nM to 10 μM) were added to a mixture of equal parts of nPA_{83} K563C*488 and nPA_{83} K563C*594 (12−150 nM), and increases in FRET were monitored over time by the 615 nm/525 nm fluorescence emission ratio. Recorded kinetic transients were fitted to eq 2 (second-order kinetics) to recover k_a (Figure 4A), and the observed rates were plotted versus the concentration of LF_N (Figure 4C). Because LF_N has been shown to promote PA_{63} oligomerization in solution, we expected that raising the LF_N concentration would increase the observed association rate, and indeed this was observed at relatively low concentrations of LF_N. However, as the LF_N concentration was raised above 50 nM, the observed oligomerization rate declined. In contrast, significant differences in observed rates were not observed for a 10-fold difference in nPA_{83} concentration, suggesting that the rate-determining step in association does not directly involve PA_{63} (Figure 4C).

Association Kinetics of $[PA_{63}]_2$·LF_N. To investigate the basis of this phenomenon, we studied the assembly of a ternary complex containing an equimolar ratio of LF_N and each of two nonoligomerizing mutant forms of PA_{63}. Mogridge et al. described D512K as a point mutation on one face of PA_{63} that blocked self-association of the protein; and a set of three mutations (K199E, R468A, and R470D) on the complementary oligomerization surface of the protein had the same effect (*21*). Neither the single mutant nor the triple mutant alone bound LF_N, but when the two were combined in the presence of LF_N, a ternary complex containing 1 equiv of each of the three proteins was formed (*21*). In this complex, $[PA_{63}]_2$·LF_N, the single- and triple-mutant forms of PA_{63} presumably associate via their complementary, wild-type faces, with LF_N bound to them in the same way it binds to pairs of adjacent subunits within the prepore (*21*).

To create a FRET-based assay of PA_{63} self-association, we introduced the K563C mutation into both of the oligomerization-deficient mutants and labeled the single (now double) mutant with Alexa 488 and the triple (now quadruple) mutant with Alexa 546. Each preparation was nicked with trypsin, and equal parts of nPA_{83} D512K*488 and nPA_{83} K199E D468A R470D K563C*546 were mixed at concentrations between 12 and 120 nM. LF_N was then added at various concentrations to initiate dimerization of the PA_{63} mutants. The fluorescence emission ratio was recorded as a function of time, and the data were fit to eq 2 to recover k_a. As shown in Figure 4D, the association rate declined as the LF_N concentration was raised, as seen in higher LF_N concentration ranges with wild-type nPA_{83}.

Dissociation Kinetics of Double-Labeled $[(PA_{63})_2$·$LF_N]$. $[(PA_{63})_2$·$LF_N]$*FRET was diluted from 5 μM to 10 nM, and the fluorescence emission ratio (570 nm/520 nm emission, 488 nm excitation) was monitored. The kinetics transients were fit using a single-exponential decay model to recover k_d (Figure 5). The measured k_d for the $[(PA_{63})_2$·$LF_N]$*FRET was $(1.3 \pm 0.01) \times 10^{-2}$ s^{-1} ($t_{1/2}$ = 53 s), showing that dissociation was 10 000-fold faster than with the $[PA_{63}]_7$*FRET.

DISCUSSION

We have measured the kinetics of $[PA_{63}]_7$ dissociation and association in the presence of LF_N using FRET between donor and acceptor fluorophores introduced into PA_{83}. Because PA_{83} contains no Cys residues, we used mixtures of Cys mutants (K563C) labeled with either Alexa fluor 488 (donor), Alexa fluor 546 (acceptor), or Alexa fluor 594 (acceptor) in our experiments. The K563C mutation has been shown not to affect activity of PA_{83} (*25*). From the $[PA_{63}]_7$ crystallographic structure, the distance between adjacent K563 residues is ~59 Å. Because the Förster distance for these two dyes was estimated to be 55 Å, FRET is an effective reporter of PA_{63} oligomerization (*22*). We also made kinetic measurements of PA_{63}·PA_{63} dissociation and association using the $[(PA_{63})_2$·$LF_N]$ construct (PA_{83} D512K and PA_{83} K199E R468A R470D) in the presence of LF_N. We expect that the distance between the adjacent K563 residues in the $[(PA_{63})_2$·$LF_N]$ complex is similar to that in the $[PA_{63}]_7$ complex, such that FRET effectively monitors its association state. Because the FRET labels were on PA_{63} and not LF_N, we monitored only the PA_{63} dissociation.

Disassembly of $[PA_{63}]_7$ was very slow, with a k_d of ~10^{-6} s^{-1}. A 10 000-fold faster dissociation rate, ~10^{-2} s^{-1}, was observed for the PA_{63} dimer bridged by LF_N. The markedly slower dissociation rate of the heptamer presumably results

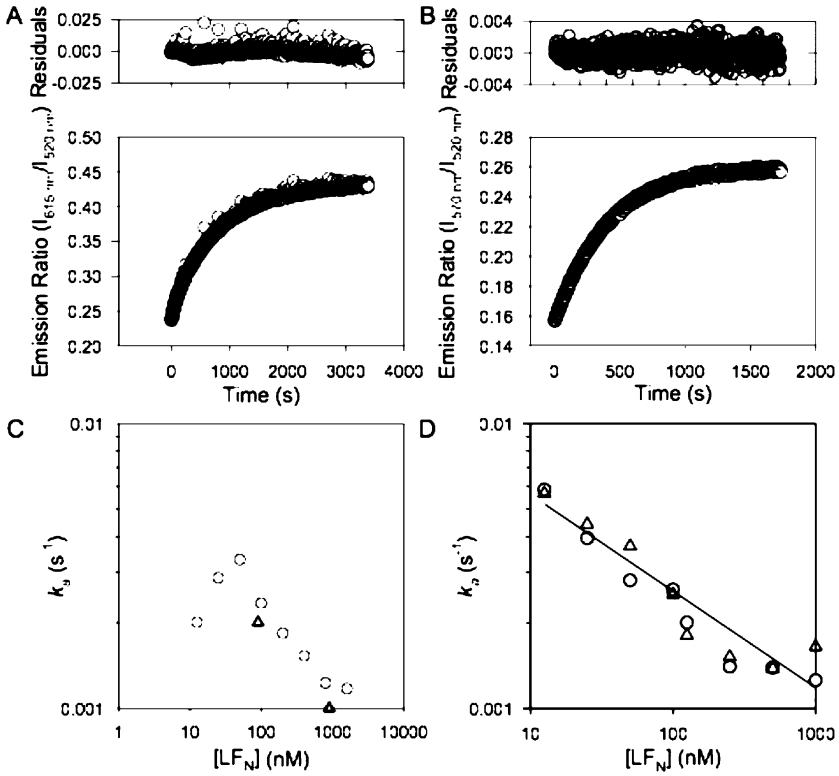

FIGURE 4: Determination of the association rates for $[PA_{63}]_7$*FRET and $[(PA_{63})_2 \cdot LF_N]$*FRET. (A) Representative data for oligomerization of PA_{63} in the presence of LF_N. LF_N (100 nM) was added at $t = 0$ to an equimolar mixture of nPA_{83} K563C*488 and nPA_{83} K563C*594 (12 nM total nPA_{83}). The increase in FRET due to PA_{63} association was monitored by fluorescence emission ratio. Data were fit to a second-order model (eq 2). Residuals are shown in the upper plot. (B) Representative data for the dimerization of nonoligomerizing PA_{83} mutants in the presence of LF_N. LF_N (100 nM) was added at $t = 0$ to an equimolar mixture of nPA_{83} D512K K563C*488 and nPA_{83} K199E R468A R470D K563C*546 (12 nM nPA_{83} total). The increase in FRET due to the association of PA_{63} was monitored by fluorescence emission ratio. Data were fit to a second-order model. Residuals are shown in the upper plot. (C) Graph of observed rate constant (k_a) for PA_{63} association versus concentration of LF_N. Circles represent data for 12 nM nPA_{83}; triangles represent data for 150 nM nPA_{83}. (D) Graph of observed rate constant (k_a) for PA_{63} dimerization of nonoligomerizing PA_{83} mutants. Circles represent data for 12 nM nPA_{83}; triangles represent data for 120 nM nPA_{83}. Data are fit by linear regression (solid line, 12 nM nPA_{83}; dotted line, 120 nM nPA_{83}).

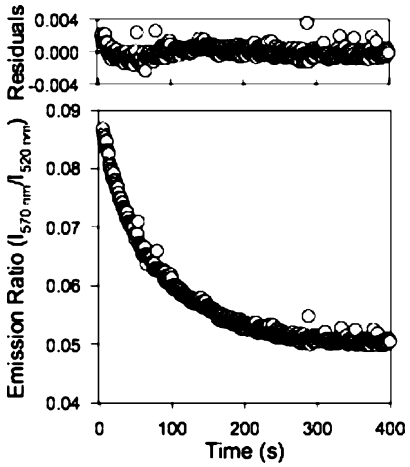

FIGURE 5: Dissociation of $[(PA_{63})_2 \cdot LF_N]$. $[(PA_{63})_2\ LF_N]$*FRET was rapidly diluted from 5 μM to a final concentration of 10 nM. A decrease in FRET was monitored over time by measuring the fluorescence emission ratio (lower plot; 570 nm/520 nm, 488 nm excitation). All data were fitted to a single-exponential decay model to recover k_d. Residuals were plotted (upper plot). Kinetic transients were acquired at 20 °C.

from cooperative interactions of each subumit with neighboring subunits in the homoheptameric ring. We surmise that the slower dissociation rate of the PA_{63} heptamer translates into a substantially increased thermodynamic stability of the heptamer relative to individual PA_{63} dimer interactions.

The substantial stability of $[PA_{63}]_7$ is of more than theoretical interest, as it impinges on the ability of dominant-negative mutant forms of PA to serve as potent antitoxins and, hence, as potential therapeutics for treating anthrax infections. Certain point mutations in the pore-forming domain (domain 2) of PA block the ability of the $[PA_{63}]_7$ prepore to undergo the conformational transition to the pore (e.g., D425A) or else block the translocation activity of the pore, once it is formed (e.g., F427A) (*26*, *27*). A subset of the mutant forms of PA were found to be dominant-negatives (DN), such that co-oligomerization of low stoichiometric ratios of mutant to wild-type PA yielded inactive prepores or pores. This DN phenotype depends not only on the co-oligomerization of mutant PA_{63}, with wild-type being stochastic, but also on the stability of the prepore, which precludes subunit−subunit exchange that might allow wild-type PA_{63} subunits to recombine to form uniformly wild-type heptamers.

Determination of association rates for PA_{63} is complicated by the intrinsic affinity of PA_{20} and its ability, when bound, to block self-association of PA_{63}. In cells, when membrane-bound nPA_{83} molecules dissociate to PA_{20} and PA_{63}, the PA_{63} is constrained to the two-dimensional membrane surface, whereas the PA_{20} is free to dissociate into extracellular solution. As a result, the concentration of PA_{63} in the membrane is effectively elevated relative to that of PA_{20}, and this may facilitate PA_{63} oligomerization. The picture is

Scheme 1. Oligomerization of PA_{63} in the Presence of LF_N

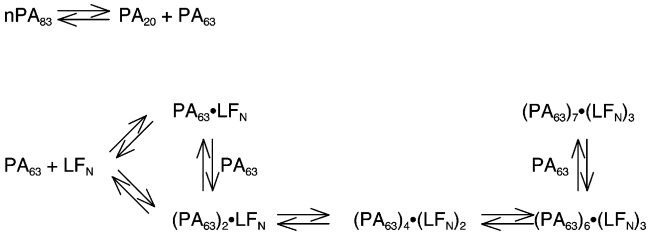

somewhat different in solution, where, except at submicromolar concentrations, PA_{20} and PA_{63} remain associated via non-covalent interactions. In this case, oligomeric PA_{63} does not exist at any measurable concentrations without the addition of at least one of the ancillary proteins: LF, LF_N (N-terminal binding domain of LF), or EF (*20*). Our working hypothesis is that in solution, LF (or LF_N) prompts oligomerization by binding to PA_{63} and preventing it from associating with PA_{20}.

We made association rate measurements of $[(PA_{63})_7 \cdot (LF_N)_3]$ and $[(PA_{63})_2 \cdot LF_N]$ using donor and acceptor labeled mixtures of nPA_{83} with variable LF_N concentrations. Unlike the measured k_d values, only small differences (factor of 2) were observed between the k_a values for $[(PA_{63})_7 \cdot (LF_N)_3]$ and $[(PA_{63})_2 \cdot LF_N]$. Notably, the observed association rate constants decreased with increasing concentrations of LF_N. This apparently indicates that LF_N inhibits PA_{63} oligomerization at higher concentrations. The measured heptamer k_a initially increased with LF_N as expected, but then decreased at higher LF_N concentrations. The dimer k_a consistently decreased with increasing LF_N concentration. Initially we hypothesized that high LF_N concentrations selectively populated PA_{63} dimers bridged by LF_N, thereby reducing free PA_{63} concentration. Because an unliganded PA_{63} subunit is necessary to complete the $[PA_{63}]_7$ ring, this could effectively inhibit assembly of toxic complexes. However, subsequent measurements of $[(PA_{63})_2 \cdot LF_N]$ k_a also demonstrated a negative dependence on LF_N concentration, indicating the existence of another or competing source of the observed rate decreases.

Consistent with these data, we propose the mechanism shown in Scheme 1 to account for the observed rate behavior. In this case, oligomerization would proceed through formation of PA_{63} dimers bridged by LF_N (similar to the $[(PA_{63})_2 \cdot LF_N]$ complex), and $PA_{63} \cdot LF_N$ complex formation would be a competing pathway that inhibits heptamer formation. At high LF_N concentrations, closing the heptamer ring structure could not proceed without dissociation of LF_N from PA_{63} and is not favored. In addition, because the observed k_a is independent of nPA_{83} concentration, binding of PA_{63} to LF_N must occur only after a rate-determining unimolecular rearrangement of LF_N.

Because our proposed mechanism predicts the existence of a $[PA_{63} \cdot LF_N]$ species, we attempted to detect this species using FRET. We titrated nPA_{83} D512K K563C*488 with LF_N E126C labeled with Alexa fluor 594 (LF_N E126C*594) and also measured dissociation of the putative [LF_N E126C*594·PA_{63} D512K K563C*488] by rapid dilution of the complex while measuring the fluorescence emission ratio (data not shown). Although significant populations of FRET complex were not detected, these data do not rule out the existence of a $[PA_{63} \cdot LF_N]$ complex. Supposing the $[PA_{63} \cdot LF_N]$ species had a K_d of 10 μM−1 mM, accurate measurement of K_d would require such high concentrations of protein to make FRET observation unlikely. In addition, a low-affinity complex may have a very short individual lifetime and relatively fast off-rates and would not be detectable using a slow kinetic approach. The complex could also be oriented such that the donor−acceptor distance approaches or exceeds twice the Förster distance, making complex association or dissociation invisible to FRET measurement. Hence, although we are currently unable to observe this interaction, we assert that the most likely mechanism for LF_N-mediated oligomerization of PA_{63} is one in which both the $[PA_{63} \cdot LF_N]$ and $[(PA_{63})_2 \cdot LF_N]$ intermediates may precede or compete with $[PA_{63}]_7$. A $LF_N \cdot LF_N$ interaction could contribute to the observed negative rate dependence, but no precedent exists for such an interaction. Thus, we propose that the overpopulation of putative $[(PA_{63})_2 \cdot LF_N]$ and $[PA_{63} \cdot LF_N]$ intermediates may be the source of the observed LF_N-dependent slowing of PA_{63} oligomerization.

ACKNOWLEDGMENT

K.A.C. thanks P. C. Ackroyd for help in the preparation and evaluation of the manuscript. We also thank R.-A.L. Pimental for help with protein production and purification. R.J.C. holds equity in PharmAthene, Inc.

REFERENCES

1. Smith, H. (2000) Discovery of the anthrax toxin: the beginning of in vivo studies on pathogenic bacteria. *Trends Microbiol. 8*, 199−200.
2. Smith, H., and Stoner, H. B. (1967) Anthrax toxic complex. *Fed. Proc. 26*, 1554−1557.
3. Duesbery, N. S., Resau, J., Webb, C. P., Koochekpour, S., Koo, H. M., Leppla, S. H., and Vande Woude, G. F. (2001) Suppression of ras-mediated transformation and inhibition of tumor growth and angiogenesis by anthrax lethal factor, a proteolytic inhibitor of multiple MEK pathways. *Proc. Natl. Acad. Sci. U.S.A. 98*, 4089−4094.
4. Pellizzari, R., Guidi-Rontani, C., Vitale, G., Mock, M., and Montecucco, C. (2000) Lethal factor of *Bacillus anthracis* cleaves the N-terminus of MAPKKs: analysis of the intracellular consequences in macrophages. *Int. J. Med. Microbiol. 290*, 421−427.
5. Vitale, G., Pellizzari, R., Recchi, C., Napolitani, G., Mock, M., and Montecucco, C. (1998) Anthrax lethal factor cleaves the N-terminus of MAPKKs and induces tyrosine/threonine phosphorylation of MAPKs in cultured macrophages. *Biochem. Biophys. Res. Commun. 248*, 706−711.
6. Bradley, K. A., Mogridge, J., Mourez, M., Collier, R. J., and Young, J. A. (2001) Identification of the cellular receptor for anthrax toxin. *Nature 414*, 225−229.
7. Scobie, H. M., Rainey, G. J., Bradley, K. A., and Young, J. A. (2003) Human capillary morphogenesis protein 2 functions as an anthrax toxin receptor. *Proc. Natl. Acad. Sci. U.S.A. 100*, 5170−5174.
8. Klimpel, K. R., Molloy, S. S., Thomas, G., and Leppla, S. H. (1992) Anthrax toxin protective antigen is activated by a cell surface protease with the sequence specificity and catalytic properties of furin. *Proc. Natl. Acad. Sci. U.S.A. 89*, 10277−10281.
9. Molloy, S. S., Bresnahan, P. A., Leppla, S. H., Klimpel, K. R., and Thomas, G. (1992) Human furin is a calcium-dependent serine endoprotease that recognizes the sequence Arg-X-X-Arg and efficiently cleaves anthrax toxin protective antigen. *J. Biol. Chem. 267*, 16396−16402.
10. Petosa, C., Collier, R. J., Klimpel, K. R., Leppla, S. H., and Liddington, R. C. (1997) Crystal structure of the anthrax toxin protective antigen. *Nature 385*, 833−838.

11. Elliott, J. L., Mogridge, J., and Collier, R. J. (2000) A quantitative study of the interactions of *Bacillus anthracis* edema factor and lethal factor with activated protective antigen. *Biochemistry 39*, 6706−6713.
12. Mogridge, J., Cunningham, K., and Collier, R. J. (2002) Stoichiometry of anthrax toxin complexes. *Biochemistry 41*, 1079−1082.
13. Abrami, L., Liu, S., Cosson, P., Leppla, S. H., and van der Goot, F. G. (2003) Anthrax toxin triggers endocytosis of its receptor via a lipid raft-mediated clathrin-dependent process. *J. Cell Biol. 160*, 321−328.
14. Blaustein, R. O., Koehler, T. M., Collier, R. J., and Finkelstein, A. (1989) Anthrax toxin: channel-forming activity of protective antigen in planar phospholipid bilayers. *Proc. Natl. Acad. Sci. U.S.A. 86*, 2209−2213.
15. Milne, J. C., and Collier, R. J. (1993) pH-dependent permeabilization of the plasma membrane of mammalian cells by anthrax protective antigen. *Mol. Microbiol. 10*, 647−653.
16. Krantz, B. A., Trivedi, A. D., Cunningham, K., Christensen, K. A., and Collier, R. J. (2004) Acid-induced unfolding of the amino-terminal domains of the lethal and edema factors of anthrax toxin. *J. Mol. Biol. 344*, 739.
17. Zhang, S., Finkelstein, A., and Collier, R. J. (2004) Evidence that translocation of anthrax toxin's lethal factor is initiated by entry of its N terminus into the protective antigen channel. *Proc. Natl. Acad. Sci. U.S.A. 101*, 16756−16761.
18. Zhang, S., Udho, E., Wu, Z., Collier, R. J., and Finkelstein, A. (2004) Protein translocation through anthrax toxin channels formed in planar lipid bilayers. *Biophys. J. 87*, 3842−3849.
19. O'Brien, J., Friedlander, A., Dreier, T., Ezzell, J., and Leppla, S. (1985) Effects of anthrax toxin components on human neutrophils. *Infect. Immun. 47*, 306−310.
20. Christensen, K. A., Krantz, B. A., Melnyk, R. A., and Collier, R. J. (2005) Interaction of the 20 kDa and 63 kDa fragments of the anthrax toxin protective antigen: kinetics and thermodynamics. *Biochemistry 44*, 1047−1053.
21. Mogridge, J., Cunningham, K., Lacy, D. B., Mourez, M., and Collier, R. J. (2002) The lethal and edema factors of anthrax toxin bind only to oligomeric forms of the protective antigen. *Proc. Natl. Acad. Sci. U.S.A. 99*, 7045−7048.
22. Wigelsworth, D. J., Krantz, B. A., Christensen, K. A., Lacy, D. B., Juris, S. J., and Collier, R. J. (2004) Binding stoichiometry and kinetics of the interaction of a human anthrax toxin receptor, CMG2, with protective antigen. *J. Biol. Chem. 279*, 23349−23356.
23. Bernard, A., and Payton, M. (2004) *Production of Recombinant Proteins*, Wiley, New York.
24. Wesche, J., Elliott, J. L., Falnes, P. O., Olsnes, S., and Collier, R. J. (1998) Characterization of membrane translocation by anthrax protective antigen. *Biochemistry 37*, 15737−15746.
25. Mourez, M., Yan, M., Lacy, D. B., Dillon, L., Bentsen, L., Marpoe, A., Maurin, C., Hotze, E., Wigelsworth, D., Pimental, R. A., Ballard, J. D., Collier, R. J., and Tweten, R. K. (2003) Mapping dominant-negative mutations of anthrax protective antigen by scanning mutagenesis. *Proc. Natl. Acad. Sci. U.S.A. 100*, 13803−13808.
26. Krantz, B. A., Melnyk, R. A., Zhang, S., Juris, S. J., Lacy, D. B., Wu, Z., Finkelstein, A., and Collier, R. J. (2005) A phenylalanine clamp catalyzes protein translocation through the anthrax toxin pore. *Science 309*, 777−781.
27. Sellman, B. R., Mourez, M., and Collier, R. J. (2001) Dominant-negative mutants of a toxin subunit: an approach to therapy of anthrax. *Science 292*, 695−697.

BI051830Y